MAGNETIC RESONANCE

Role of MRI in the early diagnosis of tubal ectopic pregnancy

Ming-Jue Si[1] · Shuang Gui[1] · Qin Fan[2] · Hong-Xiu Han[3] · Qian-Qian Zhao[3] ·
Zhi-Xin Li[1] · Jiang-Min Zhao[1]

Abstract

Objective To determine the role of MRI in the early diagnosis of tubal ectopic pregnancy (EP).

Methods Clinical and MRI features of 27 cases of tubal pregnancy were reviewed.

Results A thick-walled gestational sac (GS)-like structure was demonstrated lateral to the uterus in all cases. On T2-weighted images, the thick wall typically exhibited 3 discrete rings in 22 cases (81 %), among which 17 cases (63 %) displayed small vessels and 6 cases (33 %) exhibited small areas of fresh haemorrhage inside the thick wall. The contents demonstrated non-specific liquid in 26 %, papillary solid components in 56 %, and fresh blood or fluid-fluid level in 19 % of the cases. Dilatation of the affected fallopian tube associated with hematosalpinx was demonstrated in 18 cases (67 %) and marked enhancement of the tubal wall was observed in 22 cases (81 %). No correlation was found between the size of the GS and the estimated gestational age ($r=0.056$).

Conclusion MRI plays an important role in the early diagnosis and management of tubal pregnancy. The characteristic MRI features include a GS-like structure with a "three rings" appearance on T2-weighted images, presence of solid components in the sac, dilatation of the affected fallopian tube with hematosalpinx, and tubal wall enhancement.

Key Points
• *MR imaging has served as a problem-solving procedure in ectopic pregnancy.*
• *MR imaging features can be criteria for early diagnosis of tubal pregnancy.*
• *Detailed assessment of ectopic implantation is necessary for management decision-making.*

Abbreviations
EP   Ectopic pregnancy
US   Ultrasound
GS   Gestational sac

✉ Jiang-Min Zhao
zhaojiangmin1962@hotmail.com

Ming-Jue Si
smjsh@hotmail.com

Shuang Gui
guishuang.good@163.com

Qin Fan
122697070@qq.com

Hong-Xiu Han
715376158@qq.com

Qian-Qian Zhao
373054676@qq.com

Zhi-Xin Li
lizhixin2000@163.com

[1]   Department of Radiology, Shanghai No. 9 People's Hospital, Affiliated to Shanghai Jiao Tong University School of Medicine, No.280, Mohe Road, Shanghai 201900, China

[2]   Department of Gynecology-Obstetrics, Shanghai No. 9 People's Hospital, Affiliated to Shanghai Jiao Tong University School of Medicine, No.280, Mohe Road, Shanghai 201900, China

[3]   Department of Pathology, Shanghai No. 9 People's Hospital, Affiliated to Shanghai Jiao Tong University School of Medicine, No.280, Mohe Road, Shanghai 201900, China

Introduction

Ectopic pregnancy (EP), which accounts for approximately 2 % of all pregnancies, is the implantation of a fertilized ovum outside the uterine cavity [1]. The most common location for EP is the fallopian tube, accounting for 97 % of the cases [2]. EP is a life-threatening surgical emergency and a leading cause of maternal mortality during the first trimester of pregnancy [1, 3]. However, the mortality associated with EP has significantly decreased over the past two decades due to the advancements in early diagnosis and treatment [1]. When the EP is detected in early stages with a small gestational sac (GS), a conservative treatment is possible with methotrexate (MTX) or salpingostomy instead of total salpingectomy, which preserves fertility for future pregnancies.

Ultrasound (US) plays a major role in the evaluation of EP. Until recently, most EP diagnoses have been based on the pelvic US along with quantitative measurement of β-human chorionic gonadotropin (β-hCG) [2, 4–6]. However, if the GS is small without embryocardia-beats, a mixed extrauterine mass is detected via US, which is inconclusive for the diagnosis of EP. Moreover, if the patient is in the early stages of EP and requires conservative treatment, a detailed evaluation of the GS and the affected fallopian tube is necessary to help clinicians make proper management decisions. In these situations, magnetic resonance imaging (MRI) is being increasingly used as a problem-solving imaging modality adjunct to US [3, 5, 7]. Further, MRI provides additional information for complicated EP that facilitates the determination of appropriate management in a timely manner [5, 7].

To the best of our knowledge, only a few studies focusing on MRI for EP have been conducted. Additionally, most of the studies were limited to case reports or parts of the review series [3–5, 7–9], wherein the characteristic MRI features were not extensively discussed. In this study, we retrospectively reviewed the MR images of 27 cases of tubal EP. The purpose of the study was to determine the role of MRI in the early diagnosis and management of EP, and to investigate the characteristic MRI features with respect to the pathological findings.

Materials and methods

Patients

Between January 2012 and October 2014, we retrospectively reviewed the medical records, US, and MRI results of 27 patients who were clinically suspected of having EP at our institution. The mean age of the patients was 29.2±5.4 years old (range: 18–43 years). Mean estimated gestational age at diagnosis (based on the last menstrual period) was 6.5±0.8 weeks (range: 5–8 weeks). All the patients were hemodynamically stable with 89 % (24/27) complaining of mild to moderate lower abdominal pain, 78 % (21/27) presenting vaginal spotting, and 11 % (3/27) being asymptomatic at the time of presentation. Serum β-hCG values measured before MR examination was obtained for all patients (range: 219–23200 mIU/mL, mean: 8301 mIU/mL).

All the patients underwent a surgical procedure [surgery, laparoscopy, or dilatation and curettage (D&C)] and the final diagnosis of tubal EP was histopathologically confirmed. The fallopian tube was integral or slightly ruptured in 24 cases of which 22 cases were located in the ampulla (81 %, 22/27) and 2 cases in the interstitial region (7 %, 2/27). The fallopian tube was completely ruptured in 3 cases, all of which were located in the isthma (11 %, 3/27). Total salpingectomy was performed in nice patients, among which five patients were further analyzed for imaging features with respect to the pathological findings.

Written informed consent for contrast-enhanced MRI was obtained from all the patients. The institutional review board approved this study whilst consent for the retrospective analysis was waived by the board. The indication of contrast-enhanced MRI on patients with suspected EP was as follows: 1. The patient was β-hCG positive, hemodynamically stable, and intrauterine pregnancy was excluded without massive bloody ascites on US; 2. The patient desired fertility preservation and preferred conservative treatment to maximally preserve fertility; 3. The diagnosis of early EP was inconclusive by US, or was definitive by US with the prospect of conservative treatment, which needed more accurate evaluation by MRI. The contraindication was as follows: 1. The patient was hypotensive with massive vaginal bleeding and severe abdominal pain indicative of EP rupture, which required emergency surgery; 2. The diagnosis of EP was definite based on β-hCG level and US, and the patient had no requirement of conservative treatment; 3. The patient had general contraindications to the MR examination, such as an intrauterine device (IUD), implantation of cardiac pacemaker or metal prosthesis, severe renal dysfunction, epilepsy, asthma and/or claustrophobia.

MRI techniques

MRI was performed on a 1.5-T unit (Signa; GE Medical Systems, Milwaukee, WI) using an 8-channel phased-array coil. Images were obtained from the level of the umbilicus to the symphysis pubis. The sequences of MRI studies are summarized in Table 1.

Unenhanced MRI sequences included: (1) axial T1-weighed fast spin-echo imaging [echo time (TR)/repetition time (TE)=400–450/10–15 ms; section thickness=5 mm; intersection gap=1.5 mm; field of view=320 mm; matrix=

Table 1   MRI protocol for patients suspected of having EP

Imaging sequence and plane	TR (msec)/TE (msec)	Section thickness (mm)	Intersection gap (mm)	Field of view (mm)	Matrix	Number of acquisitions
T1-weighted FSE (27 cases)						
-Axial	400–450/10–15	5	1.5	320	320×240	4
T2-weighted FRFSE (27 cases)						
-Axial with fat-suppression	3500–4000/100–130	5	1.5	320	320×240	4
-Coronal with fat-suppression	3500–4000/100–130	5	1	260	288×192	2
-Sagittal	3500–4000/100–130	5	1	260	288×192	2
DWI (19 cases)	4000/64	6	2	320	128×128	4
3D Fiesta GRE (5 cases)	3.4–3.5/1.6–1.7	6	0	380	224×224	1
Coronal CUBE T2-weighted FSE (3 cases)	2000/91–95	1.6	0	240	228×228	1
Contrast-enhanced T1-weighted LAVA with fat-suppression (27 cases)						
-Axial	400–450/10–15	5	1	260–320	256×256	_
-Coronal	400–450/10–15	5	1	260–320	288×192	_
-Sagittal	400–450/10–15	5	1	260–320	288×192	_

Note: TR = time of repetition, TE = time of echo, FSE = fast spin-echo, FRFSE = fast recovery fast spin echo, GRE = gradient-echo, LAVA = liver acquisition with volume acceleration

320×240; number of excitations=4)]; (2) axial, coronal, and sagittal T2-weighted fast recovery fast spin echo imaging with or without fat suppression (TR/TE=3500–4000/100–130 ms; section thickness=5 mm; intersection gap=1–1.5 mm; field of view=260–320 mm; matrix=288×192–320×240; number of acquisitions=2 or 4) were performed on all 27 cases; (3) diffusion-weighted imaging (b=700) was performed on 19 cases; (4) axial, coronal, and sagittal T2-weighted gradient-echo 3D Fiesta imaging was performed on 5 cases (TR/TE= 3.4–3.5/1.6–1.7 ms; section thickness=6 mm; intersection gap=0 mm; field of view=380 mm; matrix=224×224; number of acquisitions=1); and (5) coronal T2-weighted fast spin-echo CUBE imaging was performed on 3 cases (TR/TE= 2000/91–95 ms; section thickness=1.6 mm; intersection gap=0 mm; field of view=240 mm; matrix=228×228; number of acquisitions=1).

Contrast-enhanced T1-weighted liver acquisition with volume acceleration (LAVA) imaging with fat-suppression was performed on all the 27 cases following a rapid intravenous injection of a 0.1-mmol/kg dose of gadopentetate dimeglumine (Magnevist; Schering [now Bayer Health-Care]) in the axial, coronal, and sagittal planes (TR/TE=400–450/10–15 ms; section thickness= 5 mm; intersection gap=1 mm; field of view=260– 320 mm; matrix=288×192–256×256).

The contrast-enhanced MRI should be performed only when the normal intrauterine pregnancy is excluded by US and reconfirmed by unenhanced MR sequences. Otherwise, gadolinium-based contrast agents should be avoided.

MRI image analysis

All images were reviewed retrospectively and independently by two radiologists with more than five years of experience in interpreting obstetric MRI. The MRI findings of all cases were categorized and recorded. Any disagreement was resolved by discussion to arrive at a consensus. The MRI findings were categorized as: extrauterine GS-like structure (size and shape, wall and content, signal intensities, and enhancement pattern); changes in the affected fallopian tube (tubal dilatation, hematosalpinx, and tubal wall enhancement); and presence of blood ascites. Endometrial and ovarian abnormalities were also evaluated. The extrauterine GS-like structure was defined as a sac-like cystic structure surrounded by a thick wall, which was similar to that observed via sonography [3, 5, 10]. MRI signal intensities were compared with those of the myometrium on both T1- and T2-weighted images. The degree of contrast enhancement was graded mild, moderate, or marked relative to that of the myometrium.

Statistical analysis

The 'Statistical Package for the Social Sciences' (SPSS), version 19.0, was used for data description and analysis. Spearman's correlation analysis was performed to determine the correlation coefficient (r) between the size of the GS and estimated gestational age. $P<0.05$ was considered to denote a statistically significant difference.

Results

The MRI features of 27 patients with tubal EP are summarized in Table 2.

Extrauterine GS-like structure

A well-demarcated and thick-walled cystic mass presumed to be a GS was demonstrated lateral or adjacent to the uterus in all the cases (100 %). The shape was round in 12 cases (44 %) and oval in 15 cases (56 %). The maximum diameter of the sac ranged from 10–43 mm [mean±standard deviation (SD): 22.5 ±10.1 mm]. The thickness of the wall ranged from 2.5–6.6 mm (mean±SD: 4.7±1.0 mm).

The thick wall of the GS-like structures displayed hyper-signal-intensity relative to the myometrium in 59 % of cases (16/27; Figs. 3a and 4a), iso-signal-intensity in 33 % of cases (9/27; Fig. 1a), and slightly hypo-signal-intensity in 8 % of cases (2/27; Fig. 2a) on T1-weighted images (T1-WIs). On T2-weighted images (T2-WIs), the thick wall typically exhibited 3 discrete rings in 81 % of cases (22/27): the outer and inner rings were thin and hypointense, whereas the middle ring was thick and slightly hyperintense (Figs. 1b–d, 2b–d, and 3b). Dot-like or linear low-signal intensities inside the thick middle ring on T2-WIs, which was clearer on T2-weighted CUBE images (Figs. 1d, 2c and 5c), indicated small vessels within the thick wall in 17 cases (63 %, 17/27). Six cases (33 %, 6/27) exhibited small areas with distinct hyper-signal-intensities on T2-WIs and iso- to hyper-signal-intensities on T1-WIs, together suggesting fresh haemorrhage inside the wall. Diffusion-weighted imaging (DWI) was performed on 19 cases. The thick wall displayed heterogeneous hyper-signal-intensities in all the cases (100 %; 19/19; Figs. 3d and 4d), whereas hypo-signal-intensities were observed in 84 % of cases (16/19, Fig. 4d) and hyper-signal-intensities in 16 % of cases (3/19, Fig. 3d). After administration of contrast material, the thick wall exhibited a marked and heterogeneous enhancement pattern (Figs. 1e–f, 2f–g, 3e–f, and 4g–h).

The contents of the GS-like structures in all the cases were divided into three types: 26 % of cases (7/27) exhibited non-specific liquid with hypo-signal-intensity on T1-WIs and hyper-signal-intensity on T2-WIs without enhanced solid components (Figs. 4a–h); 56 % of cases (15/27) exhibited papillary solid components representing embryo tissues with iso-signal-intensity on a T2-WI and marked enhancement (Figs. 1e, 3e–f and 5a–f); and 19 % of cases (5/27) exhibited hyper-signal-intensities on both T1- and T2-WIs, indicating fresh blood (Fig. 2a–d and g) or a fluid-fluid level resulting from blood degradation without a visible solid component (Fig. 6).

Changes in the fallopian tube

Dilatation of the affected fallopian tube associated with a clot of hyper-signal- intensities on T1-WIs and mixed on T2-WIs and consistent with hematosalpinx (Figs. 1h–i, 2b, e, and 3g) was observed in 67 % of cases (18/27). After the administration of contrast material, 81 % of cases (22/27) exhibited marked enhancement of the tubal wall (Figs. 2f–g, 3g, and 4g–h).

Isolated hemoperitoneum

Forty-one % of cases (11/27) demonstrated a small to moderate amount of hemoperitoneum, and 11 % of cases (3/27) with a completely ruptured fallopian tube demonstrated a moderate to large amount of hemoperitoneum in the pelvic cavity with signal intensities higher than that of urine in the bladder on T1-WIs (Figs. 1a–b and 2a–b). Twenty-two % of cases (6/27) exhibited a small amount of clear fluid with hypo-signal-intensity on T1-WIs and hyper-signal-intensity on T2-WIs in the pelvic cavity.

Table 2 MRI features of 27 cases of tubal EP

Features	
Size of GS-like structures (mm)	13–43 (25±8)
Shape of GS-like structures	
-Round	12/27 (44 %)
-Oval	15/27 (56 %)
Wall of GS-like structures	
Signal intensity on T1-WI	
-Hyper	16/27 (59 %)
-Iso	9/27 (33 %)
-Hypo	2/27 (8 %)
Signal intensity on T2-WI	
-Hypo outer ring+ Hyper middle ring+ Iso inner ring	22/27 (81 %)
-Small areas of fresh hemorrhage	9/27 (33 %)
Contents of GS-like structures	
Four Types:	
-Nonspecific liquid	5/27 (19 %)
-Dot-like or treelike solid components	15/27 (56 %)
-Blood	5/27 (19 %)
-Fluid-fluid level	2/27 (7 %)
Changes of fallopian tube	
-Tube dilatation and hematosalpinx	18/27 (67 %)
-Tube enhancement	22/27 (81 %)
Ascite	
-Bloody	14/27 (52 %)
- Nonspecific liquid	6/27 (22 %)

Note: GS= gestational sac

Fig. 1 Left tubal pregnancy in a 31-year-old woman at five weeks of gestation. (a) Axial T1-weighted image reveals a cystic GS-like structure on the left side of the uterus with a thick wall of iso-signal intensity and the content of hypo-signal intensity (*white arrow*). (b) Axial, (c) Coronal, (d) Sagittal T2-WIs clearly demonstrate the "three rings" appearance of the thick wall (*white arrows*). A moderate volume of free fluid with high-signal intensities on both T1- and T2-WIs is present in the pelvis, indicative of bloody ascites (*yellow asterisks*). (e) Axial, (f) and (g) Sagittal post-contrast T1-WIs with fat suppression clearly reveal a difference in enhancement patterns between the GS (*white arrows*) and a corpus luteum cyst (*black arrows*) on the left side of the GS. The former is heterogeneously enhanced with a rough thick wall and papillary solid components, while the latter displays a homogeneous enhancement pattern with a thinner and more regular wall lacking solid components. The left ovary is markedly enhanced (*black asterisk*) demonstrating the ovarian origin of the corpus luteum cyst. (h) Coronal T1- and (i) Coronal T2-WIs with fat suppression show a hyper-signal intensity clot (*dotted arrows*) in the dilated left fallopian tube consistent with hematosalpinx. The findings during surgery confirmed a slightly ruptured left tubal pregnancy

Other simultaneous findings in the 27 cases were as follows: four thin-walled decidual cysts, two apparent intrauterine haemorrhages, three uterine fibroids, and one endometriosis. Corpus luteum cysts were coexisted with EP in 6 cases (22 %; Fig. 1c, e, and g), and 5 cases (19 %) exhibited caesarean scars.

In the 24 integral or slightly ruptured cases, a GS-like structure was demonstrated lateral to the uterus which was surrounded by the adjacent fallopian tube and sometimes associated with small amount of hemoperitoneum. In contrast, in the three completely ruptured cases, a deformed GS-like structure was wrapped in a poorly defined complex hematoma in the lateral section of the uterus and was usually associated with a large amount of hemoperitoneum.

No correlation was found between the size of the GS and the estimated gestational age ($r=0.056$), thereby suggesting a delay in GS development due to abnormal implantation.

Discussion

EP is a well-known acute condition, which is associated with a 9–14 % mortality rate [1, 11]. Ninety-seven percent of the EPs occur in the fallopian tube, of which 75–80 % are located in the ampulla, 10 % in the isthma, 5 % in the fimbria, and 2–4 % in the interstitial region [2, 12]. Patients typically present at about 5–6 weeks gestational age with symptoms, such as vaginal spotting and pelvic pain [2, 6]. Symptoms of severe acute abdominal pain with heavy vaginal bleeding and hemodynamic instability indicate rupture of an EP, which requires emergent surgical intervention [13]. In recent years, progress has been made in the treatment of EP. Conservative therapies, such as systemic or local injection of MTX, laparoscopic salpingostomy, or salpingotomy, have been widely used in patients with EP to preserve fertility. However, the diagnosis of EP should be definite and the morphology of the GS, as well as the affected fallopian tube, should be evaluated prior to its management.

US remains the initial imaging modality for evaluating patients with suspected EP. Numerous signs and US criteria in the diagnosis of EP have been described in the literature [2, 6, 14, 15]. The most specific US criterion of EP is the presence of an extrauterine GS with either a yolk sac or embryo, with 100 % specificity if embryocardia beats are detected. However, this criterion has limited sensitivity (15–20 %) [16], owing to high operator dependency and interference by intervening bowel gas, heavy haemorrhage, or coexistence of an ovarian
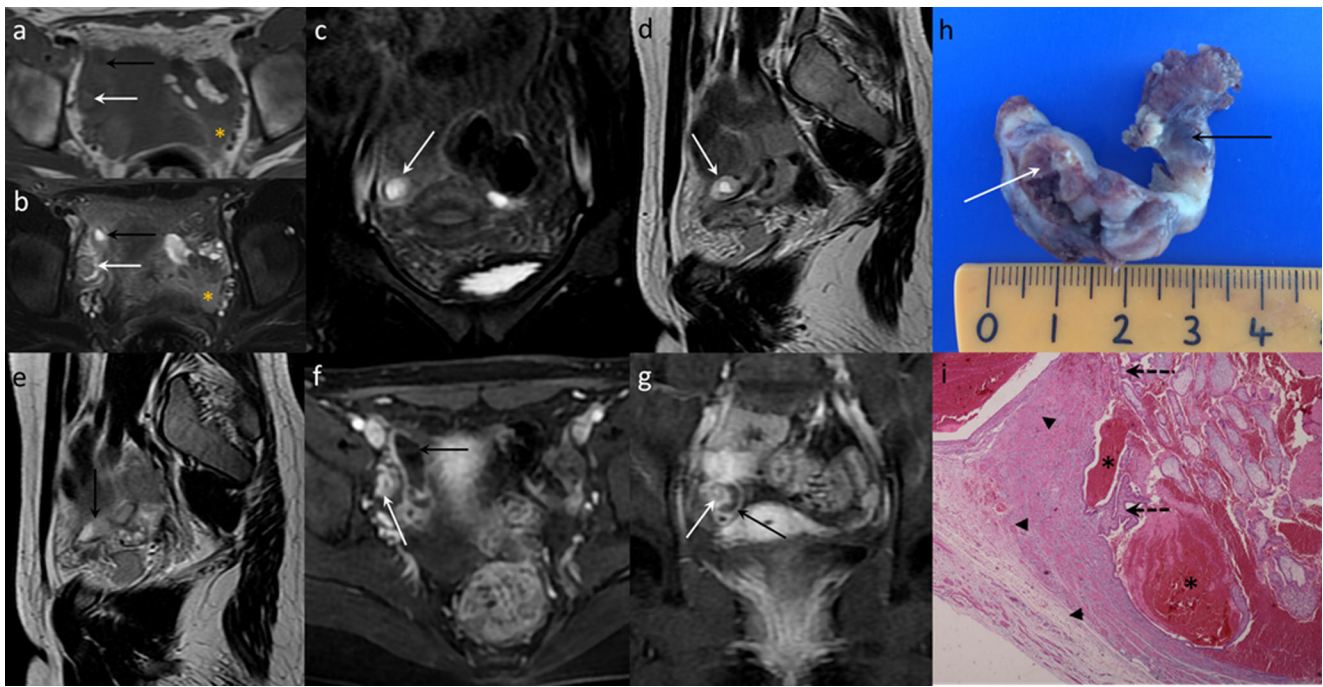
Fig. 2 Right tubal pregnancy in a 23-year-old woman at 6 weeks of gestation. (a) Axial T1- and (b) T2-WIs demonstrate a GS-like structure lateral to the uterus with a component of hyper-signal intensity on both T1- and T2-WIs, which is indicative of blood (*white arrows*). A small amount of free fluid with a slightly increased intensity on T1-WI is present in the pelvis consistent with bloody ascites (*asterisk*). On (c) coronal and (d) sagittal T2-WIs, the thick wall of the GS exhibits a "three rings" appearance (*white arrows*). (a)(b)(e) The adjacent right fallopian tube is dilated with a fluid-fluid level resulting from degradation of hematosalpinx (*black arrows*). (f) Axial and (g) coronal T1-WIs with fat suppression reveal that both the wall of the GS (*white arrows*) and the dilated tubal wall (*black arrows*) are markedly enhanced after administration of contrast material. (h) Gross specimen shows that the proximal fallopian tube wraps a thick-walled GS-like structure (*white arrow*) and the distal fallopian tube is dilated by haemorrhage (*black arrow*). (i) Photomicrograph (haematoxylin-eosin, 40×) demonstrates that the tubal wall (*arrow heads*) is thick and invaded by the trophoblastic villus (*black dotted arrows*), resulting in abundant interstitial haemorrhage (*asterisks*)

mass, which results in non-visualization of the implantation site of the EP in up to 15–35 % of the cases [6, 15]. Since accurate localization and a detailed assessment of GS are particularly important for conservative laparoscopic surgery or medical therapy with MTX [10], MRI has been used as a problem-solving adjunct to US for early diagnosis and accurate evaluation of EP prior to its management [10, 17]. The advantages of MRI include excellent soft tissue contrast, a large field of view, multi-planar imaging capability, and sensitivity to identify fresh blood [5, 17–19].

To our knowledge, only a few studies focusing on MRI for EP have been conducted [3–5, 7, 8, 10]. Parker RA III et al. [17] reported that the MRI findings of EP included a heterogeneous adnexal mass composed of GS, hematosalpinx, and bloody ascites. Ha HK et al. [20] reported that the post-contrast MR images might provide better delineation of GS as a hemorrhagic mass with enhanced, tree-like, solid components in EP cases. However, the role of MRI in the evaluation of EP has not been defined and the characteristic MRI features have not been fully investigated.

We have demonstrated that the most characteristic MRI feature of EP is the cystic lesion with a thick wall typically exhibiting a "three rings" appearance on T2-WIs with or without solid components. This appearance is rarely observed in other adnexal masses, thus, it can be used as a key imaging feature. The pathological examination showed that the thick middle ring was composed of chorionic villi tissue, which contained abundant fetal capillaries and maternal blood in the interstitium, thereby resulting in hyper-signal-intensity on T2-WIs and marked enhancement after administration of contrast material. The thin outer ring was formed by the adjacent tubal wall, whereas the thin inner ring was formed by extraembryonic coelom and amnion without blood vessels, thereby resulting in hypo-signal-intensities on T2-WIs. Some of the previous studies reported small areas of hemorrhage in the thick wall of GS; however, in this study, only 33 % of the cases presented punctuated intramural bleeding, but nearly two-thirds of the cases displayed dot-like or linear low-signal intensities inside the thick middle ring relative to abundant fetal capillaries in the villous interstitium. In the large GS, solid components were detected on the MRI. The components were found to be composed of embryo tissue upon pathological examinations. In cases with no visible solid components, but only fresh blood or fluid-fluid level on the MRI, the US could not detect embryocardia beats, which indicated death of the embryo due to wrong implantation.
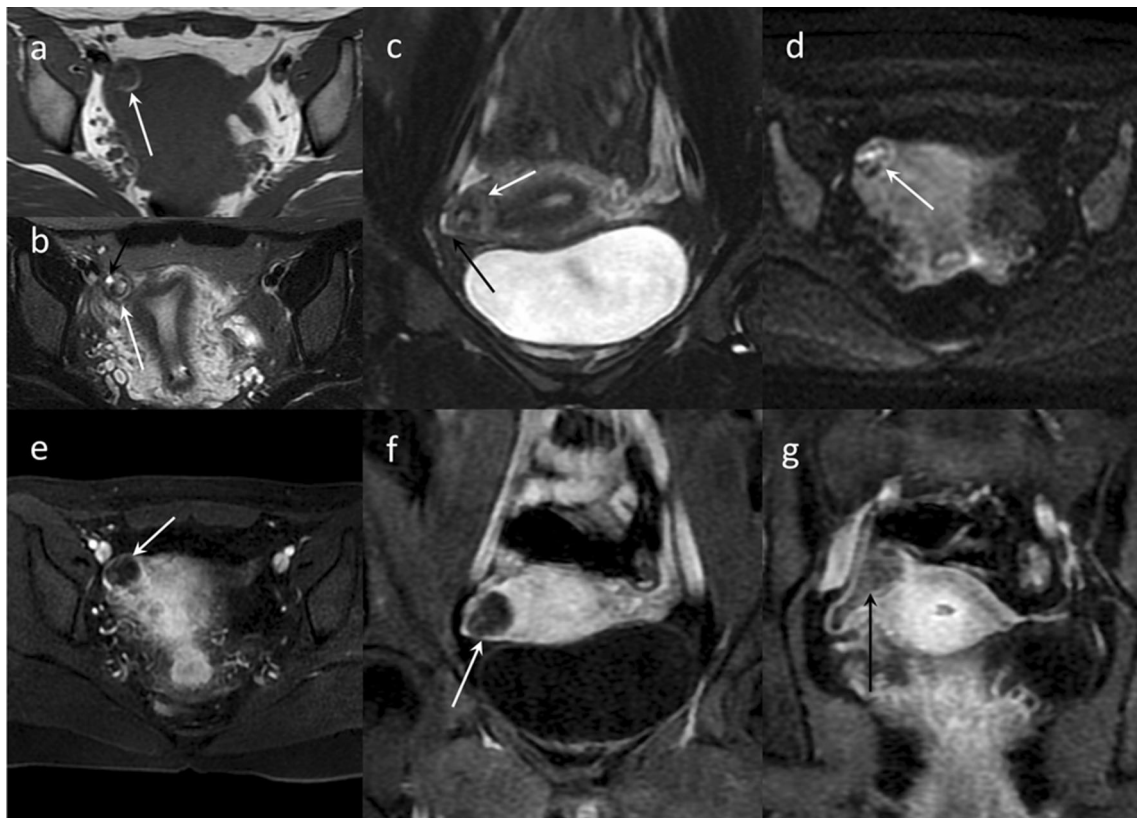
Fig. 3 Right tubal pregnancy in a 27-year-old woman at 6 weeks of gestation. The US demonstrates a possible "cornual" EP: (a) Axial T1-, (b) axial T2-, and (c) coronal T2-WIs demonstrate a GS-like structure located lateral to the right horn and the uninterrupted junctional zone. The wall reveals hyper-signal intensity on the T1-WI and a "three rings" appearance on the T2-WI (*white arrows*) with a small fluid-fluid level in the centre. The surrounding fallopian tube is dilated (*black arrows*). Note the uterus is arcuate-shaped and empty. (d) A diffusion-weighted image reveals the GS with the wall of heterogeneous iso-signal intensity and the component of high-signal intensity (*white arrow*). (e) Axial and (f) coronal enhanced T1-WIs with fat suppression reveal dense enhancement of the p0eriphery with enhancing papillary components (*white arrows*). (g) A coronal enhanced T1-WI also exhibits a significant dilatation of the affected right tube with marked enhancement of the wall and heterogeneous blood in the lumen (*black arrow*). The findings at surgery helped confirm an un-ruptured EP in the interstitial region of the right fallopian tube

The changes in the affected fallopian tube were also helpful in the diagnosis of EP, including tubal dilatation with hematosalpinx and tubal wall enhancement on contrast enhanced MR images. Pathological examination showed that the adjacent tubal wall was penetrated by chorionic villi and trophoblasts to form the placenta following the implantation of the ovum in the tubal epithelium. This resulted in rupture of the intramural arterioles and bleeding into the tubal lumen, consequently leading to hematosalpinx [3, 10, 17]. MRI is more effective in evaluating minor changes in the affected fallopian tube as compared to US.

Isolated bloody ascites have been reported as important indicators of EP [3]. In the present study, 11 % of the cases exhibited a moderate to large amount of bloody ascites in the pelvis due to complete rupture of the affected fallopian tube and 41 % of the cases demonstrated a small amount of hemoperitoneum, which might be due to the effusion of intraluminal blood from the opening of fimbria. However, MRI is much more sensitive than US in detecting small amounts of free liquid and identifying bloody ascites from simple pelvic fluid.

MRI is a valuable and indispensable technique for the assessment of tubal EP: (1) axial and coronal T2-WI: although sagittal T2-WI is used as a basic MR sequence in gynaecological emergencies [21], axial and coronal T2-wighted imaging is more helpful in EP cases to investigate the relationship between GS, myometrium, and the dilated fallopian tube; (2) T1-WI: is effective in identifying blood in the adnexal masses and hemoperitoneum in the pelvic cavity. Acute to sub-acute haemorrhage generally appears as iso- to hyper-signal-intensity on T1-WIs and mixed on T2-WIs [17]; (3) contrast-enhanced sequences: allow a highly specific diagnosis of tubal pregnancy by demonstrating a GS-like structure or fresh hematoma surrounded by the enhancing tubal wall; (4) T2-weighted 3D Fiesta and CUBE imaging: allows more accurate identification of the borderline and the solid components of the GS even in the presence of surrounding hematoma. In one of our cases, the CUBE imaging clearly
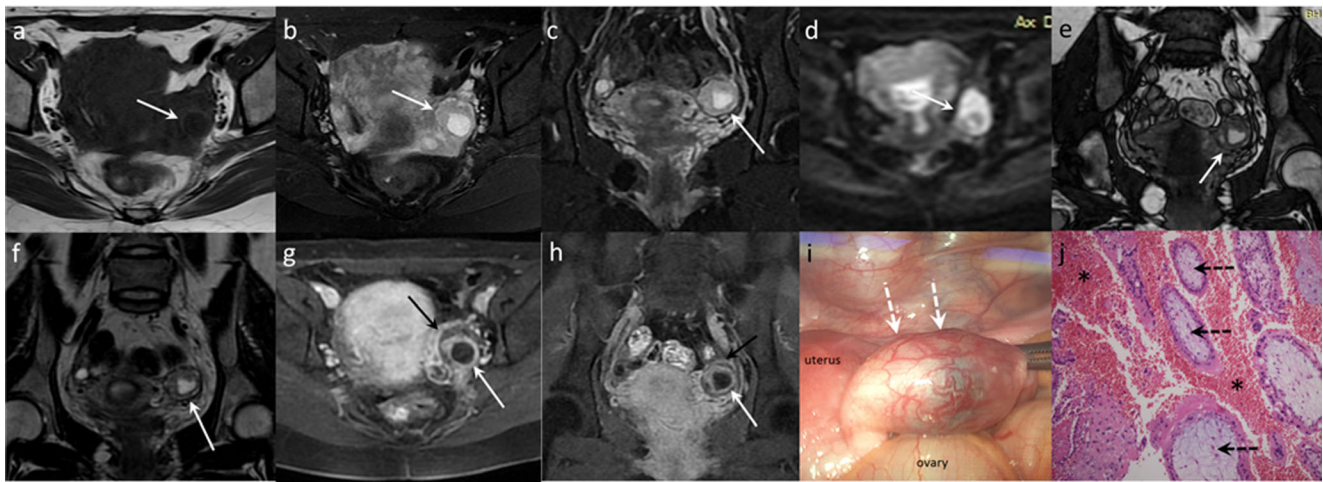
Fig. 4 Left tubal pregnancy in a 26-year-old woman at 6 weeks of gestation. (a) Axial T1-, (b) axial T2-, and (c) coronal T2-WIs display a left GS-like structure, which is surrounded by a thick wall of slightly hyper-signal intensity on both T1- and T2-WIs (*white arrows*). The component exhibits similar-signal intensity to that of simple fluid without visible embryo tissue on a T2-WI. (d) On a diffusion-weighted image, the wall of the GS demonstrates hyper-signal intensity and components of hypo-signal intensity (*white arrow*). (e) Coronal T2-weighted 3D Fiesta and (f) coronal T2-weighted CUBE images clearly displayed the borderline between the GS and the adjacent tubal wall as well as their relationships with the uterus (*white arrows*). (g) Axial and (h) coronal post-contrast T1-WIs with fat suppression demonstrate the GS with ring-like enhancement (*white arrows*) associated with prominent tubal wall enhancement (*black arrows*), which allows definitive diagnosis of tubal pregnancy. (i) Laparoscopy reveals a sausage-shaped distention of the left fallopian tube with a dark red serosal surface (*white dotted arrows*). (j) Photomicrograph (haematoxylin-eosin, 200×) of the tubal mass demonstrates chorionic villi (*black dotted arrows*) with haemorrhage (*asterisks*)
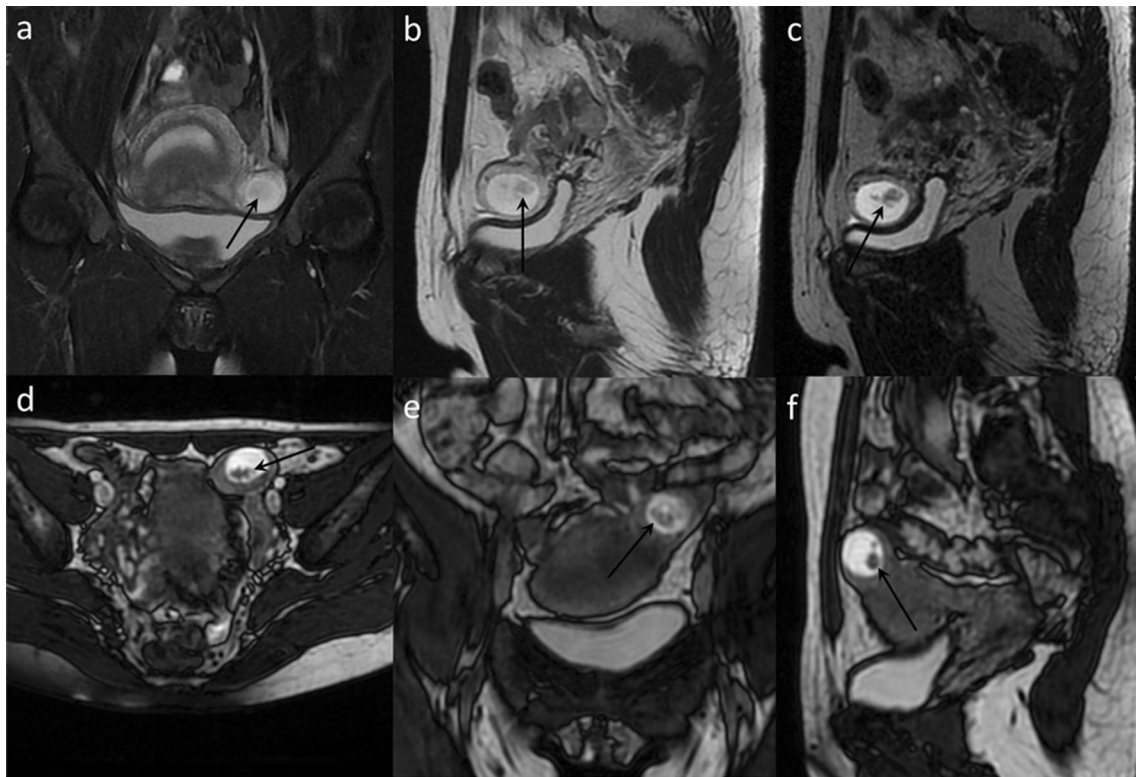
Fig. 5 Left tubal pregnancy in a 29-year-old woman at 8 weeks of gestation. (a) Coronal T2-WI with fat suppression and (b) sagittal T2-WI display a GS-like structure located slightly lateral to the left horn of uterus. The component exhibits hyper-signal intensity with possible solid components (*black arrows*). (c) Sagittal T2-weighted CUBE image, (d) axial, (e) coronal, and (f) sagittal T2-weighted 3D Fiesta images clearly demonstrate that the solid component has a fetal shape (*black arrows*). The relationship between the GS, adjacent tubal wall, and uterus is clearly demonstrated on these unconventional MR sequences
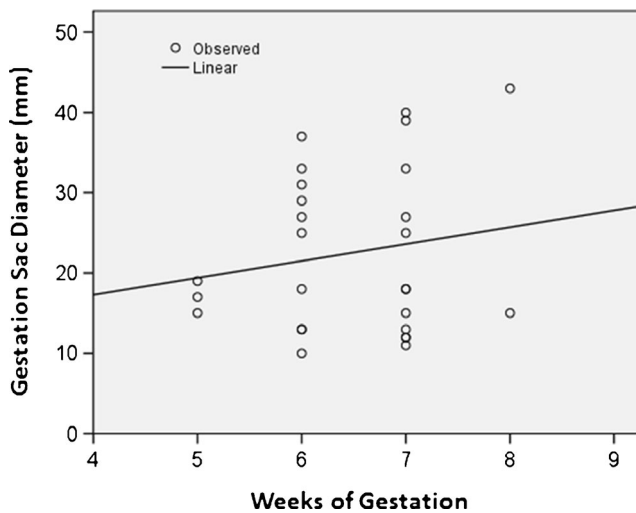
Fig. 6 The correlation between the estimated gestational age and the GS size

demonstrated that the solid component of the GS had a fetal shape in a tubal pregnancy at 8 weeks of gestation. CUBE imaging can also reveal the intramural vessels of the GS and the vessels beside the uterus. The drawback associated with CUBE imaging is the long acquisition time, thus, it should be reserved for clinically and hemodynamically stable patients.

The main distinguishing feature of tubal EP diagnosis is the presence of a corpus luteum cyst or theca lutein cyst associated with pregnancy, exhibiting a similar thick-walled cystic appearance. A corpus luteal cyst is the most common ovarian mass in the first trimester of pregnancy; however, most of these are spontaneously regressed by the end of the second trimester [22]. Theca lutein cysts develop in response to high levels of β-hCG, which is commonly found in patients with hydatidiform moles, or secondary to overstimulation of the ovaries by clomiphene or gonadotropins [23]. Both corpus luteum and theca lutein cysts originate from the ovary where EPs in the ovary are exceedingly rare [24]. On MRI, the GS of EP typically exhibits a "three rings" appearance on a T2-WI with a rough thick wall often containing small areas of haemorrhage and small vessels. After administration of contrast material, the wall is heterogeneously enhanced with or without enhanced solid components. The corpus luteum cyst usually demonstrates a thinner and more regular wall with slightly hyper-signal intensity on T1-WIs and relatively hypo-signal intensity on T2-WIs, and displays a more homogeneous enhancement pattern without solid components [25]. The theca lutein cysts usually appear as multiple, variably sized cystic lesions in bilaterally symmetric, enlarged ovaries with relatively thin walls and do not exhibit acute haemorrhage [10, 26]. In addition, cystic ovarian neoplasms can sometimes occur during pregnancy and can be difficult to distinguish from EP on the basis of imaging alone. The tumour marker measurement could be helpful in this context.

Our study has several limitations. First, it was a retrospective study and included a relatively small sample size of tubal EP. In order to confirm the diagnostic accuracy of MRI features and statistical significance, more cases should be included in future studies. Second, the majority of the cases (89 %) were associated with an un-ruptured or slightly ruptured EP, and the MRI features of completely ruptured EPs were not fully discussed. This condition is a life-threatening surgical emergency and is difficult to manage for a long-time examination like MRI. The suspicion of tubal rupture more often depends on the clinical settings, including acute severe abdominal pain, guarding and rebound tenderness at physical examination, hemodynamic instability, and dropping hematocrit [10]. Third, EP frequently coexists with a corpus luteum cyst with differences in origination and morphology. However, when the lesions are tiny, it can be very difficult to discriminate between them by MRI.

Conclusion

MRI plays an important role in the early diagnosis of tubal pregnancy and provides accurate evaluation of the lesion to help make management decisions. Radiologists should choose the most necessary MRI sequences according to the requirements. The characteristic MR features include a GS-like structure with a "three rings" appearance on T2-WIs, presence of solid components in the sac, dilatation of the affected tube with hematosalpinx, and tubal wall enhancement.

References

1. Centers for Disease Control and Prevention CDC (1995) Ectopic pregnancy: United States, 1990-1992. MMWR Morb Mortal Wkly Rep 44:46–48
2. Dialani V, Levine D (2004) Ectopic pregnancy: a review. Ultrasound Q 20:105–117
3. Takahashi A, Takahama J, Marugami N et al (2013) Ectopic pregnancy: MRI findings and clinical utility. Abdom Imaging 38:844–850
4. Kinoshita T, Ishii K, Higashiiwai H (1999) MR appearance of ruptured tubal ectopic pregnancy. Eur J Radiol 32:144–147

5. Kataoka ML, Togashi K, Kobayashi H et al (1999) Evaluation of ectopic pregnancy by magnetic resonance imaging. Hum Reprod 14:2644–2650

6. Lin EP, Bhatt S, Dogra VS (2008) Diagnostic clues to ectopic pregnancy. Radiographics 28:1661–1671

7. Nishino M, Hayakawa K, Kawamata K et al (2002) MRI of early unruptured ectopic pregnancy: detection of gestational sac. J Comput Assist Tomogr 26:134–137

8. Yoshigi J, Yashiro N, Kinoshita T et al (2006) Diagnosis of ectopic pregnancy with MRI: efficacy of T2*-weighted imaging. Magn Reson Med Sci 5:25–32

9. Bourdel N, Roman H, Gallot D et al (2007) Interstitial Pregnancy. Ultrasonographic diagnosis and contribution of MRI. A case report. Gynecol Obstet Fertil 35:121–124

10. Tamai K, Koyama T, Togashi K (2007) MR features of ectopic pregnancy. Eur Radiol 17:3236–3246

11. Lozeau AM, Potter B (2005) Diagnosis and management of ectopic pregnancy. Am Fam Physician 72:1707–1714

12. Breen JL (1970) A 21 year survey of 654 ectopic pregnancies. Am J Obstet Gynecol 106:1004–1019

13. Attar E (2004) Endocrinology of ectopic pregnancy. Obstet Gynecol Clin North Am 31:779–794

14. Kao LY, Scheinfeld MH, Chernyak V et al (2014) Beyond ultrasound: CT and MRI of ectopic pregnancy. AJR Am J Roentgenol 202:904–911

15. Levine D (2007) Ectopic pregnancy. Radiology 245:385–397

16. Brown DL, Doubilet PM (1994) Transvaginal sonography for diagnosing ectopic pregnancy: positivity criteria and performance characteristics. J Ultrasound Med 13:259–266

17. Parker RA 3rd, Yano M, Tai AW et al (2012) MR imaging findings of ectopic pregnancy: a pictorial review. Radiographics 32:1445–1460

18. Singh AK, Desai H, Novelline RA et al (2009) Emergency MRI of acute pelvic pain: MR protocol with no oral contrast. Emerg Radiol 16:133–141

19. Nagayama M, Watanabe Y, Okumura A et al (2002) Fast MR imaging in obstetrics. Radiographics 22:563–580

20. Ha HK, Jung JK, Kang SJ et al (1993) MR imaging in the diagnosis of rare forms of ectopic pregnancy. AJR Am J Roentgenol 160:1229–1232

21. Filhastre M, Dechaud H, Lesnik A et al (2005) Interstitial pregnancy: role of MRI. Eur Radiol 15:93–95

22. Horton KM, Tempany CMC (1995) MRI in pregnancy. In: Tempany CMC (ed) MR and imaging of the female pelvis. Mosby, St. Louis, pp 201–219

23. Ha HK (1999) Computed tomography and magnetic resonance imaging of pathologic conditions of pregnancy. In: Anderson JC (ed) Gynecologic imaging. Churchill Livingstone, London, pp 443–450

24. Grimes HG, Nosal RA, Gallagher JC (1983) Ovarian pregnancy: a series of 24 cases. Obstet Gynecol 61:174–180

25. Tamai K, Koyama T, Saga T et al (2006) MR features of physiologic and benign conditions of the ovary. Eur Radiol 16:2700–2711

26. Jung SE, Byun JY, Lee JM et al (2001) MR imaging of maternal diseases in pregnancy. AJR Am J Roentgenol 177:1293–1300